*Int. J. Electrochem. Sci.*, 14 **(2019)** 7220 – 7231, doi: 10.20964/2019.08.09

International Journal of
ELECTROCHEMICAL
SCIENCE
www.electrochemsci.org

# Synergistic Effects of Light Rare Earth Element and Gd on the Electrochemical Performances of $Ce_2Ni_7$-type La-Mg-Ni-based Alloys

*Zhijie Gao*[1,*], *Xiangyang Shi* [2], *Ke Xin*[3], *Yumeng Ma* [4]

[1] Department of Chemical Engineering and Safety, Binzhou University, Binzhou 256600, PR China
[2] Flight College, Binzhou University, Binzhou 256600, PR China
[3] College of Information Engineering, Binzhou University, Binzhou 256600, PR China
[4] College of Aeronautical Engineering, Binzhou University, Binzhou 256600, PR China
[*]E-mail: gaozhijie1983@126.com

*Received:* 5 April 2019 / *Accepted:* 27 May 2019 / *Published:* 30 June 2019

The influences of light rare earth element and Gd substitution for La on the phase structures, and electrochemical properties of $La_{0.43}R_{0.2}Gd_{0.2}Mg_{0.17}Ni_{3.1}Co_{0.3}Al_{0.1}$ (R = La, Ce, Pr, Nd, Y, Sm, Gd, Yb) alloys have been investigated. Compared to basic $La_{0.83}Mg_{0.17}Ni_{3.1}Co_{0.3}Al_{0.1}$ alloy, the alloys consist of a main $Ce_2Ni_7$-type $(RE,Mg)_2Ni_7$ phase, plus a few $Gd_2Co_7$-type phase and $CaCu_5$-type $LaNi_5$ phase. R = La promotes the formation of $Ce_2Ni_7$-type super-stacking phases. Further study shows that partial replacement of La for other rare earth elements stimulates the formation of $Gd_2Co_7$-type phase. Electrochemical analysis shows that the cycling stability for the alloy with R = La reaches 91.4% after 100 charge/discharge cycles. Meanwhile the maximum discharge capacity is improved to 389.94 mAh $g^{-1}$. We conclude that R = La increases the phase abundance of $Ce_2Ni_7$-type structure so that the discharge capacity and cycling stability are enhanced. The substitution of other rare earth elements increases the phase abundance of $Gd_2Co_7$-type so as to deteriorate the electrochemical performances. Alloys with R = La shows the optimal electrochemical performances.

**Keywords:** RE-Mg-Ni-based hydrogen storage alloy, light rare earth element and Gd substitution, Microstructure, Electrochemical properties

## 1. INTRODUCTION

$Ce_2Ni_7$-type hydrogen storage alloys of La-Mg-Ni system are determined as a new generation anode materials of nickel/metal hydride batteries because of their high discharge capacity (~410 mAh $g^{-1}$) [1, 2], superior high rate dischargeability [3], environmental friendliness [4] and other advantages

[5-12]. However, their cycle life need to be further improved to satisfy the urgent demand for a power source with favorable overall electrochemical performance.

It is well known that a large number of investigations on $Ce_2Ni_7$-type La-Mg-Ni-based alloy have been carried out [13-18]. The research on the inferior cycling stability of their alloys is still further understanding. Although the intrinsic reason for the inferior cycling stability of the alloy is not clear, the previous research has accumulated a lot of valuable information. Some important regular enlightenments have also been drawn as follows:

(1) At present, most of the annealed $Ce_2Ni_7$-type alloys in the study form multiphase structures, resulting in uneven distribution of alloy composition. The above mentioned greatly affects the study of the mechanism of action of rare earth elements, and it has also been difficult to make a correct analysis and evaluation of the electrochemical behavior and performance of single phase. (2) The atomic size of rare earth elements affects the phase transformation, structural stability and hydrogen induced amorphization (HIA) tendency of the alloys. The order of the atomic radii of rare earth elements is $r_{La} > r_{Pr} > r_{Ce} > r_{Nd} > r_{Sm} > r_{Gd}$ [11, 19]. Based on $r_A / r_B > 1.37$ ($r_A$ and $r_B$ stand for the atomic radii of the A and B elements of the $AB_n$ alloy, respectively) [20], it may have a profound effect on HIA and electrochemical properties of $Ce_2Ni_7$-type alloys by making use of partial replacement of La with rare earth elements with a smaller atomic radii. (3) Magnesium is a key element in the La-Mg-Ni-based alloys [21, 22]. The Mg content has a significant effect on the hydrogenation/dehydrogenation behavior of La-Mg-Ni based alloys [7, 23]. By adjusting the content of low Mg combined with rare earth elements, it may be an important way to further improve the cycling stability of $Ce_2Ni_7$-type alloy electrode.

In addition, Li et al. [24] used Gd and Mg to substitute for La in $La_{0.8-x}Gd_xMg_{0.2}Ni_{3.15}Co_{0.25}Al_{0.1}$ (x = 0-0.4) alloys and found that the abundance of the $Ce_2Ni_7$-type phase increased with the increasing amount of Gd. The increase of the $Ce_2Ni_7$-type phase abundance tremendously developed the cycling stability of $Ce_2Ni_7$-type alloy electrode. The co-substitution of Gd and Mg for La improved the overall electrochemical properties of $Ce_2Ni_7$-type alloy. It can clearly be seen that the co-substitution method not only overcomes the deficiencies brought by a single element but also achieves the multi-function effect owing to the cooperation of various elements. Rare earth elements render tremendous influence in the cycling stability of $Ce_2Ni_7$-type alloys due to the fact that they are the actual hydrogen absorption/desorption elements. Therefore, the co-substitution method of rare earth elements is supposed to be promising on $Ce_2Ni_7$-type alloys, but this has hardly been reported so far.

Based on the discussion above, in this study, light rare earth elements and Gd are used to partially substitute for La in $La_{0.43}R_{0.2}Gd_{0.2}Mg_{0.17}Ni_{3.1}Co_{0.3}Al_{0.1}$ (R = La, Ce, Pr, Nd, Y, Sm, Gd, Yb) alloys. The effects of the co-substitution of light rare earth elements and Gd on the phase evolution and electrochemical performances of the alloys are investigated. The synergistic effects of light rare earth elements and Gd have been illustrated. It is expected that a proper amount of light rare earth elements and Gd substitution for La can effectively ameliorate the overall electrochemical performances, especially the cycling stability of the $Ce_2Ni_7$-type La-Mg-Ni-based alloys.

## 2. EXPERIMENTAL DETAILS

### *2.1 Sample Preparation*

The alloys designed as $La_{0.43}R_{0.2}Gd_{0.2}Mg_{0.17}Ni_{3.1}Co_{0.3}Al_{0.1}$ (R = La, Ce, Pr, Nd, Y, Sm, Gd, Yb) were prepared by the induction melting method at 0.4 MPa of Ar atmosphere. The ingots were annealed for 8 hours at 1173 K under Ar pressure (0.1 MPa). A compensation of 5 wt.% of both rare earth elements and Mg was applied due to the burning loss. The purity of all elements was above 99.9 wt.%.

### *2.2 Structural and Electrochemical Characterization*

The annealed alloy was mechanically pulverized into powder (<38 μm) for X-ray diffraction (XRD) measurement, and 54 to 61 μm powder was used for electrode testing. XRD measurements were performed on a Rigaku D / max-2400 diffractometer with Cu radiation and 40 kV x 150 mA power. The pattern was recorded in the range of 15° to 90° in which the step size of 2θ was 0.02°. Then the collected data were analyzed by the Rietveld method [25] using Fullprof 2000 software [26] to get the lattice parameters. The backscattered electron images were obtained by making use of Electron probe micro analyzer (EPMA-1600) with wave dispersive spectroscopy (WDS), which was used to characterize the phase structure and the composition of alloys.

The annealed alloy powders of ~0.1g were selected from 54 to 61 microns and the electrodes were prepared. The alloy electrode was synthesized by cold pressing the mixture of the alloy powder and nickel carbonyl powder at a weight ratio of 1:3 under 20 MPa pressure to form anodes with a diameter of 10 mm. The electrochemical measurements were carried out at 298K in a standard open three-electrode cell. The cell consists of an alloy electrode, a sintered $Ni(OH)_2$/NiOH cathode and a Hg/HgO reference electrode immersed in 6M KOH electrolyte. Discharge each electrode to the cut-off potential -0.6 V vs. Hg/HgO reference electrode. During the activation process, the electrode was charged/discharged at a current density of 60 mA $g^{-1}$. When the cycle stability at 298 K was checked, the electrode was charged/discharged at a current density of 300 mA $g^{-1}$.

## 3. RESULTS AND DISCUSSION

### *3.1 Alloy crystal structure*

Fig. 1 shows the XRD patterns for $La_{0.43}R_{0.2}Gd_{0.2}Mg_{0.17}Ni_{3.1}Co_{0.3}Al_{0.1}$ (R = La, Ce, Pr, Nd, Y, Sm, Gd, Yb) alloys. According to the Rietveld refinement analyses, the abundance of phase and cell parameters was tabulated in Table 1. Rietveld analysis of R=La, Ce, Pr, Nd alloys is shown in Figure 2. It can be seen that all of alloys are multi-phase structures. The main phase is the $Ce_2Ni_7$-type structure. The second phase is the $Gd_2Co_7$-type phase and $CaCu_5$-type phase. From Table 1, it can be seen that the addition of Pr, Ce, Nd has no significant effect on the alloy phase structures. The phase abundance of the $Ce_2Ni_7$-type structures of these alloys is maintained at about 90 wt.%, but the addition of Gd elements has an obvious effect on it. The phase abundance of the $Gd_2Co_7$-type structure of single Gd =

0.4 substituted alloy significantly increases to 28.4 wt.% and $Ce_2Ni_7$-type structure decreases to 66.1 wt.%.

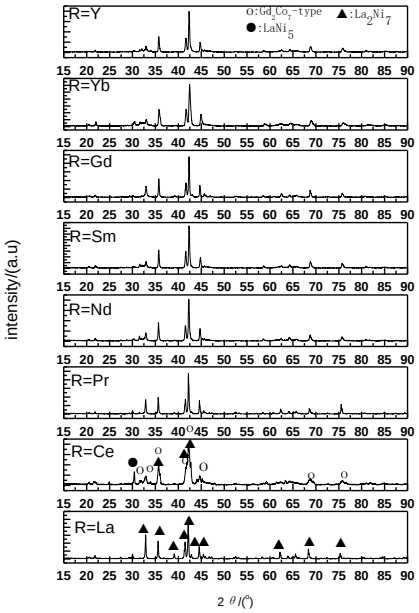


**Figure 1.** XRD patterns for $La_{0.43}R_{0.2}Gd_{0.2}Mg_{0.17}Ni_{3.1}Co_{0.3}Al_{0.1}$ (R = La, Ce, Pr, Nd, Y, Sm, Gd, Yb) alloys

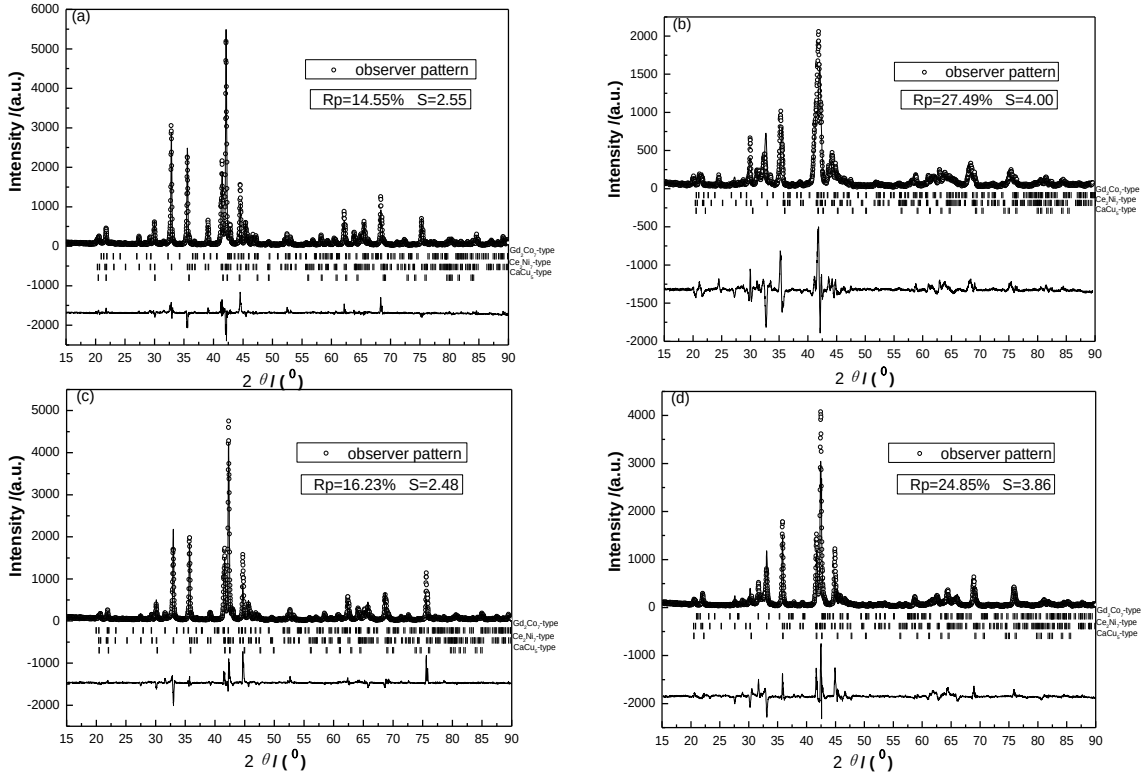


**Figure 2.** Rietveld refinement of the XRD patterns for $La_{0.43}R_{0.2}Gd_{0.2}Mg_{0.17}Ni_{3.1}Co_{0.3}Al_{0.1}$ (R = La, Ce, Pr, Nd) with R = La (a), R= Ce (b), R = Pr (c) and R = Nd (d), respectively.

**Table 1.** Characteristics of phases for $La_{0.43}R_{0.2}Gd_{0.2}Mg_{0.17}Ni_{3.1}Co_{0.3}Al_{0.1}$ alloys

| Sample | Phase | Space Group | Lattice constants (Å) | | | | Phase abundance (wt.%) |
|---|---|---|---|---|---|---|---|
| | | | a | c | V | c/a | |
| R = La | $Gd_2Co_7$ | R-3m | 4.928 | 36.496 | 767.621 | 7.41 | 0.33 |
| | $Ce_2Ni_7$ | $P6_3/mmc$ | 5.045 | 24.392 | 537.585 | 4.83 | 95.73 |
| | $CaCu_5$ | P6/mmm | 5.014 | 4.081 | 88.839 | 0.81 | 3.95 |
| R = Ce | $Gd_2Co_7$ | R-3m | 5.027 | 36.604 | 800.936 | 7.28 | 2.35 |
| | $Ce_2Ni_7$ | $P6_3/mmc$ | 5.030 | 24.412 | 534.812 | 4.85 | 83.84 |
| | $CaCu_5$ | P6/mmm | 5.000 | 4.017 | 86.977 | 0.80 | 13.81 |
| R = Pr | $Gd_2Co_7$ | R-3m | 5.169 | 36.601 | 847.024 | 7.08 | 2.14 |
| | $Ce_2Ni_7$ | $P6_3/mmc$ | 5.026 | 24.317 | 531.862 | 4.84 | 94.13 |
| | $CaCu_5$ | P6/mmm | 5.007 | 4.034 | 87.591 | 0.81 | 3.73 |
| R = Nd | $Gd_2Co_7$ | R-3m | 4.872 | 38.147 | 784.104 | 7.83 | 7.86 |
| | $Ce_2Ni_7$ | $P6_3/mmc$ | 5.013 | 24.235 | 527.413 | 4.83 | 90.76 |
| | $CaCu_5$ | P6/mmm | 5.002 | 4.001 | 86.681 | 0.80 | 1.38 |
| R = Gd | $Gd_2Co_7$ | R-3m | 4.548 | 36.290 | 673.100 | 7.98 | 28.40 |
| | $Ce_2Ni_7$ | $P6_3/mmc$ | 5.011 | 24.262 | 534.600 | 4.84 | 66.10 |
| | $CaCu_5$ | P6/mmm | 4.995 | 3.809 | 82.300 | 0.76 | 5.50 |

**Table 2.** Quantified main and interaction effects of rare earth elements on the $Ce_2Ni_7$-type phase

| Element effect | a | c | V | c/a | Abundance of $Ce_2Ni_7$-type Phase (wt.%) |
|---|---|---|---|---|---|
| $La_{0.83}$（Basic） | 5.069 | 24.543 | 546.073 | 4.84 | 52.87 [11] |
| La×Gd | -0.024 | -0.151 | -8.488 | -0.01 | +42.86 |
| Ce×Gd | -0.039 | -0.131 | -11.261 | +0.01 | +30.97 |
| Pr×Gd | -0.043 | -0.226 | -14.211 | +0.00 | +41.26 |
| Nd×Gd | -0.056 | -0.308 | -18.660 | -0.01 | +37.89 |
| $La\times Gd_{0.4}$ | -0.058 | -0.281 | -11.473 | +0.00 | +13.23 |

**Table 3.** Quantified main and interaction effects of rare earth elements on the $Gd_2Co_7$-type phase

| Element effect | a | c | V | c/a | Abundance of $Gd_2Co_7$-type Phase (wt.%) |
|---|---|---|---|---|---|
| $La_{0.83}$（Basic） | 5.068 | 36.720 | 816.815 | 7.25 | 7.75 [11] |
| La×Gd | -0.140 | -0.224 | -49.194 | +0.16 | -7.42 |
| Ce×Gd | -0.041 | -0.116 | -15.879 | +0.03 | -5.40 |
| Pr×Gd | 0.101 | -0.119 | 30.209 | -0.17 | -5.61 |
| Nd×Gd | -0.196 | 1.427 | -32.711 | +0.58 | +0.11 |
| $La\times Gd_{0.4}$ | -0.520 | -0.430 | -143.715 | +0.73 | +20.65 |

The effects of additional elements on the phase abundance of $Ce_2Ni_7$- and $Gd_2Co_7$-type phase and the interaction of light rare earth element i.e. Ce, Pr, Nd and Gd on the phase abundances of different alloys are listed in Tables 2 and 3, respectively. Compared to the $La_{0.83}Mg_{0.17}Ni_{3.1}Co_{0.3}Al_{0.1}$ basic alloy, the synergy effect of La-Gd-substitution is maximum on the phase abundance of $Ce_2Ni_7$-type structure and then La-$Gd_{0.4}$-substitution is the minimum. The former increases by 42.86 wt.% and the latter increases by 13.23 wt.%. However, the $Gd_2Co_7$-type phase abundance of La-Gd-substitution alloy decreases by 7.42 wt.% and La-$Gd_{0.4}$-substitution alloy increases by 13.23 wt.%. Furthermore, the $Ce_2Ni_7$-type phase abundance of Ce-Gd-substitution, Pr-Gd-substitution and Nd-Gd-substitution increases by 30.97 wt.%, 41.26 wt.% and 37.89 wt.%, respectively. It can be concluded that the co-substitution of Ce, Pr, Nd and Gd does not affect the $Ce_2Ni_7$-type phase abundance, but the reintroduction of Gd element can significantly reduce the $Ce_2Ni_7$-type phase abundance, which is beneficial to the formation of $Gd_2Co_7$-type phase, and the $Gd_2Co_7$-type phase abundance significantly increases. When the stoichiometric ratio of R element is 0.2, it does not significantly affect the $Ce_2Ni_7$-type phase abundance of the alloy no matter how small the radius of the rare earth atom becomes except R = Gd. When the stoichiometric ratio of R element is > 0.2, the $Ce_2Ni_7$-type phase structure significantly decreases, and the $Gd_2Co_7$-type phase also significantly increases. This is consistent with the reports in references [9] and [11].

Fig. 3 presents the back scattering electron images of the $La_{0.83}Mg_{0.17}Ni_{3.1}Co_{0.3}Al_{0.1}$ basic alloy and R = La, Gd alloys as typical examples. There are two areas in the image which are dark grey and light grey. Combining with WDS analysis and Rietveld analysis, the dark grey area (A area) can be identified as $CaCu_5$-type phase, the light grey regions (B area) can be identified as $Ce_2Ni_7$-type ($Gd_2Co_7$-type) $(RE,Mg)_2Ni_7$ phase. This is also consistent with the XRD results.

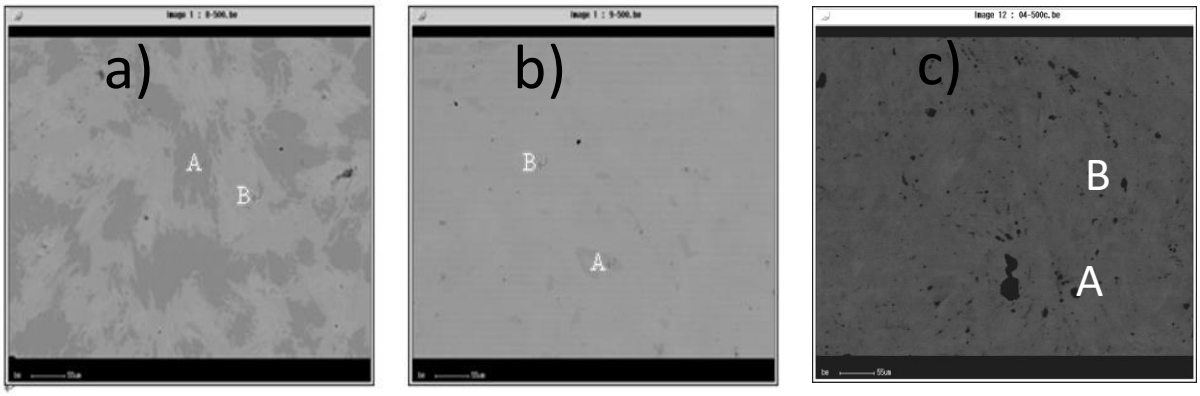


**Figure 3.** Back scattered electron images for $La_{0.83}$ (Basic) (a) and $La_{0.43}R_{0.2}Gd_{0.2}Mg_{0.17}Ni_{3.1}Co_{0.3}Al_{0.1}$ alloys: b) R = La, c) R = Gd (A: $CaCu_5$-type phase, B: $Ce_2Ni_7$-type ($Gd_2Co_7$-type) phase)

*3.2 Charge/discharge characteristics*

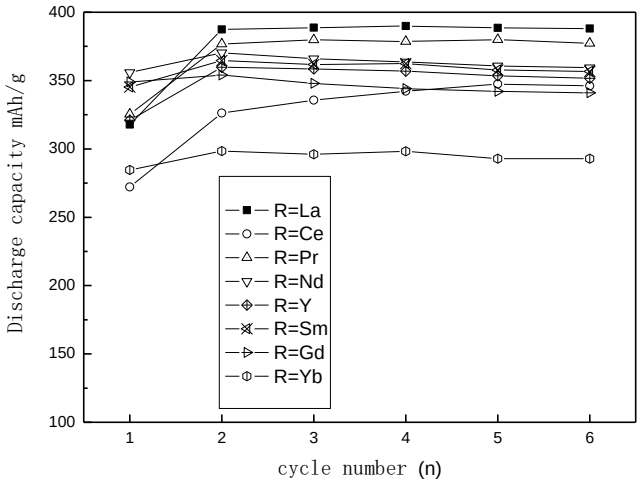


**Figure 4.** Activation curves of $La_{0.43}R_{0.2}Gd_{0.2}Mg_{0.17}Ni_{3.1}Co_{0.3}Al_{0.1}$ (R = La, Ce, Pr, Nd, Y, Sm, Gd, Yb) annealed alloy electrodes with 60 mA $g^{-1}$ charge-discharge current density at 298 K

**Table 4.** Summary of electrochemical performance for $La_{0.43}R_{0.2}Gd_{0.2}Mg_{0.17}Ni_{3.1}Co_{0.3}Al_{0.1}$ annealed alloy electrodes at 298 K

| Sample | N | $C_{max}$(mAh $g^{-1}$) | | $S_{100}$(%) |
|---|---|---|---|---|
| | | 60 mA $g^{-1}$ | 300 mA $g^{-1}$ | |
| R=Yb | 2 | 298.48 | 301.42 | 65.70 |
| R=La | 4 | 389.94 | 378.08 | 91.40 |
| R=Pr | 5 | 379.92 | 374.95 | 88.70 |
| R=Ce | 5 | 347.41 | 336.56 | 77.50 |
| R=Nd | 2 | 370.44 | 353.96 | 86.60 |
| R=Y | 2 | 359.78 | 347.17 | 81.10 |
| R=Sm | 2 | 364.68 | 354.61 | 84.80 |
| R=Gd | 2 | 354.00 | 345.00 | 78.30 |

The activation curve of the alloy electrodes at 298K is shown in Fig. 4. Table 4 lists the electrochemical performance parameters of the alloy electrodes at 298K. It can be found that the rare earth element substitution has little effect on the activation rates of the alloy electrodes. All of alloy electrodes exhibit good activation characteristics after 4 to 5 charge/discharge cycles. However, the rare earth element substitution has a significantly influence on the discharge capacity of alloy electrodes. Depending on the type of substitution element and the amount of substitution, the discharge capacity is between 298.48 mAh $g^{-1}$ and 389.94 mAh $g^{-1}$. The synergistic effect of Yb and Gd elements significantly reduces the discharge capacity of the alloy electrode, which is 298.48 mAh $g^{-1}$. The synergistic effect of La, Ce, Pr, Nd, Sm, Y and Gd elements significantly improves the discharge

capacity of the alloy electrode, respectively. The discharge capacity is 389.94, 347.41, 379.92, 370.44, 364.68 and 359.78 mAh $g^{-1}$, respectively. These results are higher than the $La_{0.83}Mg_{0.17}Ni_{3.1}Co_{0.3}Al_{0.1}$ basic alloy. But the $C_{max}$ is in the order of: La-Gd substitution > Pr-Gd substitution > Nd-Gd substitution > Sm-Gd substitution > Y-Gd substitution > single $Gd_{0.4}$ substituted alloy > $La_{0.83}$ basic alloy [11]. This is largely due to the contraction of the cell volumes, which decreases the room for hydrogen atoms.

*3.3 Cycling stability*

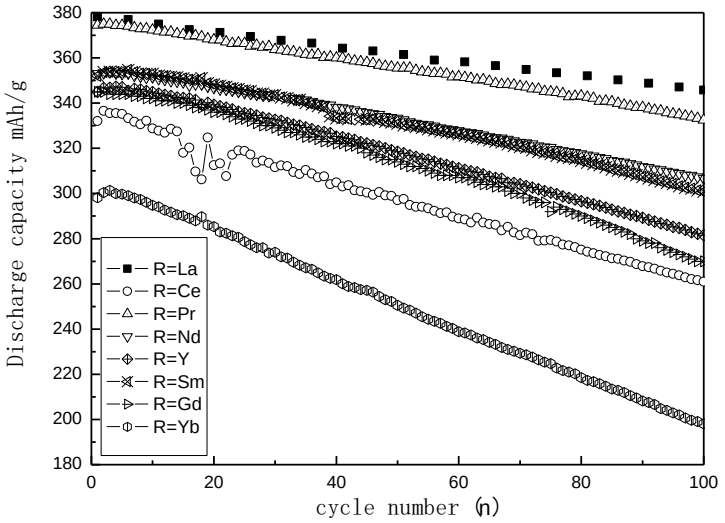


**Figure 5.** The cycling stability of $La_{0.43}R_{0.2}Gd_{0.2}Mg_{0.17}Ni_{3.1}Co_{0.3}Al_{0.1}$ (R = La, Ce, Pr, Nd, Y, Sm, Gd, Yb) annealed alloy electrodes at 298K

The $La_{0.43}R_{0.2}Gd_{0.2}Mg_{0.17}Ni_{3.1}Co_{0.3}Al_{0.1}$ (R = La, Ce, Pr, Nd, Y, Sm, Gd, Yb) alloy electrodes are subjected to 100 charge/discharge cycles. The discharge capacity retention curves are presented in Fig. 5. The cycling stability of alloy electrodes is evaluated by making use of capacity retention rate after 100 charge/discharge cycles. The capacity retention at the $100^{th}$ cycle ($S_{100}$) is defined as the ratio of $C_{100}/C_{max} \times 100\%$ (where $C_{max}$ is the maximum discharge capacity and is $C_{100}$ the discharge capacity at the $100^{th}$ cycles [19]), and is listed in Table 4. It can be found that the $S_{100}$ of all alloy electrodes varied between 91.4% and 65.7%. Compared to the $La_{0.83}Mg_{0.17}Ni_{3.1}Co_{0.3}Al_{0.1}$ basic alloy [11], the cycling stability of alloy electrodes has been improved as expected except Yb-Gd substituted alloy. From the results it is indicated that the role of light rare earth elements in $Ce_2Ni_7$-type alloy is similar with that in $AB_5$-type alloy. So, the improvement should not only result from the refinement of the alloy surface, but also be due to the change of the $Ce_2Ni_7$-type phase abundance of alloys. It is well known that corrosion is a fundamental reason for the capacity decay of the electrode alloys. The anti-corrosion capability of the alloys basically depends on rare earth elements distribution of their alloy

surface and types of phase structure [27, 28]. The order of electronegativity values of rare earth elements is Y (1.22) > Gd (1.20) > Sm (1.17) > Nd (1.14) > Pr (1.13) > Ce (1.12) > La (1.10) and it is known that partial substituting La with light rare earth elements and Gd can reduce the oxidation in KOH [29, 30]. The light rare earth elements should make contribution to the oxidation-resistance. Furthermore, the order of anti-oxidation of alloys phase is $Ce_2Ni_7$-type phase > $Gd_2Co_7$-type phase > $PuNi_3$-type phase [28, 31].

*3.4 Function of light rare earth elements and Gd in the perfectiom of electrochemical characteristics*

The electrochemical properties including $C_{max}$ and $S_{100}$ of the $La_{0.83}Mg_{0.17}Ni_{3.1}Co_{0.3}Al_{0.1}$ basic alloy, light rare earth-Gd substituted, single $Gd_{0.4}$ substituted and Yb-Gd substituted alloy electrodes are presented in Fig. 6. It can be found that the $C_{max}$ is improved by both light rare earth-Gd substitution and single $Gd_{0.4}$ substitution for La while Yb-Gd substitution cases little effect. The $C_{max}$ is in the order of: light rare earth-Gd substituted alloy > single $Gd_{0.4}$ substituted alloy > $La_{0.83}Mg_{0.17}Ni_{3.1}Co_{0.3}Al_{0.1}$ basic alloy > Yb-Gd substituted alloy. This agrees with the change in the total abundance of the $Ce_2Ni_7$-type super-stacking structures. The $S_{100}$ shown in Fig.6 is obviously developed by light rare earth-Gd substitution for La. This corresponds to the $Ce_2Ni_7$-type phase abundance and the refined alloy surface. The effect is more remarkable when La and Gd work together. It can be seen that the electrochemical results of La-Gd substituted alloy is in good accordance with the structural analysis in the part of 3.1.

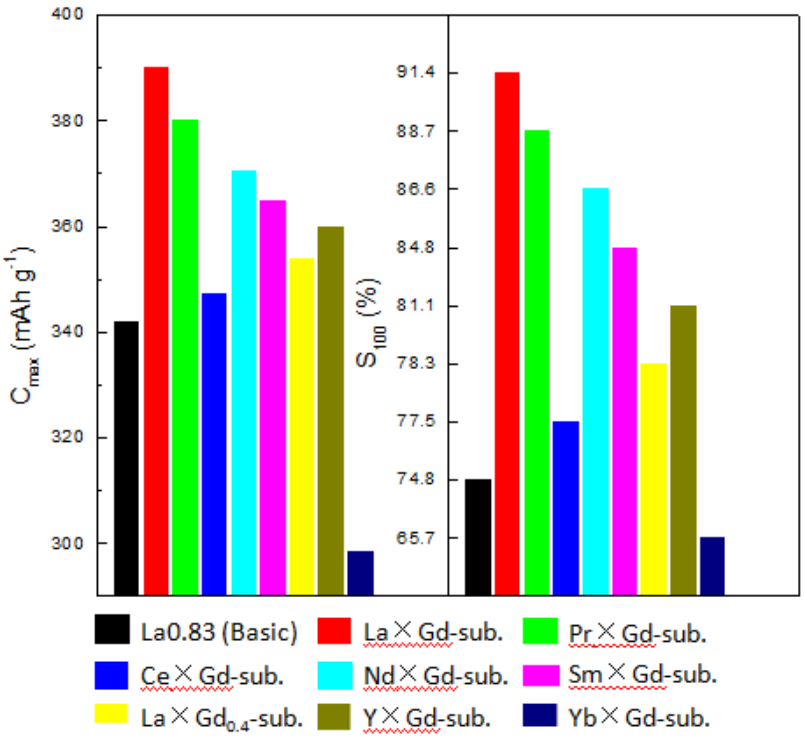


**Figure 6.** Comparison in electrochemical properties of the $La_{0.83}Mg_{0.17}Ni_{3.1}Co_{0.3}Al_{0.1}$ basic alloy, light rare earth elements-Gd substituted, single $Gd_{0.4}$ substituted, and Yb-Gd substituted alloy electrodes

The electrochemical properties including $C_{max}$ and $S_{100}$ of $La_{0.83}Mg_{0.17}Ni_{3.1}Co_{0.3}Al_{0.1}$ basic alloy [11], La-Gd substituted alloy, $La_{0.8-x}Gd_xMg_{0.2}Ni_{3.15}Co_{0.25}Al_{0.1}$ (x = 0-0.4) alloys [24] and $La_{1.5}Mg_{0.5}Ni_7$ alloy [31] are presented in Table 5. The $C_{max}$ and $S_{100}$ are in the order of: $La_{1.5}Mg_{0.5}Ni_7$ alloy ~ La-Gd substituted alloy > $La_{0.7}Gd_{0.1}Mg_{0.2}Ni_{3.15}Co_{0.25}Al_{0.1}$ alloy > $La_{0.83}Mg_{0.17}Ni_{3.1}Co_{0.3}Al_{0.1}$ basic alloy and La-Gd substituted alloy > $La_{0.7}Gd_{0.1}Mg_{0.2}Ni_{3.15}Co_{0.25}Al_{0.1}$ alloy > $La_{1.5}Mg_{0.5}Ni_7$ alloy > $La_{0.83}Mg_{0.17}Ni_{3.1}Co_{0.3}Al_{0.1}$ basic alloy, respectively. The overall electrochemical performances of La-Gd substituted alloy electrode is the best.

**Table 5.** Comparison of electrochemical performance of $La_{0.83}Mg_{0.17}Ni_{3.1}Co_{0.3}Al_{0.1}$ basic alloy [11], $La_{0.63}Gd_{0.2}Mg_{0.17}Ni_{3.1}Co_{0.3}Al_{0.1}$ alloy, $La_{0.8-x}Gd_xMg_{0.2}Ni_{3.15}Co_{0.25}Al_{0.1}$ alloys [24] and $La_{1.5}Mg_{0.5}Ni_7$ alloy [31] at 298 K

| Sample | N | $C_{max}$(mAh $g^{-1}$) | $S_{100}$(%) |
|---|---|---|---|
| $La_{0.83}Mg_{0.17}Ni_{3.1}Co_{0.3}Al_{0.1}$ [11] | 2 | 342.00 | 74.80 |
| $La_{0.63}Gd_{0.2}Mg_{0.17}Ni_{3.1}Co_{0.3}Al_{0.1}$ | 4 | 389.94 | 91.40 |
| $La_{0.8}Mg_{0.2}Ni_{3.15}Co_{0.25}Al_{0.1}$ [24] | 2 | 375.70 | 77.90 |
| $La_{0.7}Gd_{0.1}Mg_{0.2}Ni_{3.15}Co_{0.25}Al_{0.1}$ [24] | 2 | 385.20 | 82.90 |
| $La_{0.6}Gd_{0.2}Mg_{0.2}Ni_{3.15}Co_{0.25}Al_{0.1}$ [24] | 2 | 351.10 | 75.40 |
| $La_{0.5}Gd_{0.3}Mg_{0.2}Ni_{3.15}Co_{0.25}Al_{0.1}$ [24] | 2 | 313.20 | 71.30 |
| $La_{0.4}Gd_{0.4}Mg_{0.2}Ni_{3.15}Co_{0.25}Al_{0.1}$ [24] | 3 | 253.50 | 64.80 |
| $La_{1.5}Mg_{0.5}Ni_7$ [31] | 3 | 390.00 | 80.50 |

Based on the above analysis, we propose that the improvement on the discharge capacity and cycling stability of the $La_{0.43}R_{0.2}Gd_{0.2}Mg_{0.17}Ni_{3.1}Co_{0.3}Al_{0.1}$ (R = La, Ce, Pr, Nd, Y, Sm, Gd, Yb) alloys is due to the reason that light rare earth element-Gd co-substitution for La increases the $Ce_2Ni_7$-type phase abundance and decreases the $Gd_2Co_7$-type phase abundance, then the refinement in alloy surface by light rare earth element-Gd co-substitution. The La-Gd substituted alloy electrode has best the electrochemical performances of the alloy electrodes, and its discharge capacity is slightly better than the commercial $CaCu_5$-type alloy electrode.

## 4. CONCLUSIONS

The main phase of the $La_{0.43}R_{0.2}Gd_{0.2}Mg_{0.17}Ni_{3.1}Co_{0.3}Al_{0.1}$ (R = La, Ce, Pr, Nd, Y, Sm, Gd, Yb) are all indexed to be $Ce_2Ni_7$-type structure. The substitution of La by light rare earth elements-Gd has a remarkable effect on the phase structure of the alloys. Single Gd = 0.4 substitution for La is beneficial to the formation of the $Gd_2Co_7$-type phase.

1) The increase of the $Ce_2Ni_7$-type phase resulting from the substitution of light rare earth elements-Gd for La caused the improvement of anti-corrosion of the alloys and ameliorates the cycling stability of alloy electrodes.

2) All of alloy electrodes exhibit a good activation rate, and the discharge capacity is between 298.48 mAh $g^{-1}$ and 389.94 mAh $g^{-1}$ in dependence of the sort and content of substituting elements.
3) Function exploration of La and Gd co-substituted alloy indicates that La and Gd increase the phase abundance of $Ce_2Ni_7$-type super-stacking structures so that the discharge capacity and cycling stability are improved. Gd improves the anti-corrosion of the alloys surface, which enhances cycling stability. The La-Gd substituted alloy electrode has best the electrochemical performances of the alloy electrodes.

ACKNOWLEDGEMENTS
This work was supported by the Nature Science Foundation of Shandong Province (No. ZR2014EMP012, ZR2017QEE014), Doctor Foundation of Binzhou University (No. 2013Y10) and the Science and Technology Development Plan of Bingzhou (No. 2014ZC0216). The authors express sincere thanks to the NSFC (Natural Science Foundation of China, 51404220) for financial support.

**References**

1. T. Kohno, H. Yoshida, F. Kawashima, T. Inaba, I. Sakai, M. Yamamoto and M. Kanda, *J. Alloys Compd.*, 311 (2000) L5.
2. X.L. Ding, Y.T. Li, F. Fang, D.L. Sun and Q.A. Zhang, *J. Mater. Chem. A*, 5 (2017) 5067.
3. W. Lv and Y. Wu, *J. Alloys Compd.*, 789 (2019) 547.
4. K.T. Moller, T.R. Jensen, E. Akiba and H.-W. Li, *Prog. Nat. Sci.–Mater.*, 27 (2017) 34.
5. Y.T. Li, X.L. Ding, F.L. Wu, F. Fang, Q.A. Zhang and D.L. Sun, *J. Phys. Chem. C*, 120 (2016) 1415.
6. Y.T. Li, L.X. Zhang, Q.A. Zhang, F. Fang, D.L. Sun, K.Z. Li, H. Wang, L.Z. Ouyang and M. Zhu, *J. Phys. Chem. C*, 118 (2014) 23635.
7. Z.J. Gao, Y.C. Luo, R.F. Li, Z. Lin and L. Kang, *J. Power Sources*, 241 (2013) 509.
8. Y.T. Li, F. Fang, X.B. Yu, Q.A. Zhang, L.Z. Ouyang, M. Zhu and D.L. Sun, *Acta Mater.*, 59 (2011) 1829.
9. Z.J. Gao, B. Zhang, Y.C. Luo and H.-W. Li, *J. Taiwan Inst. Chem. Eng.*, 89 (2018) 183.
10. Z.J. Gao, Z.N. Yang, Y.T. Li, A.Q. Deng, Y.C. Luo and H.-W. Li, *Dalton Trans.*, 47 (2018) 16453.
11. Z.J. Gao, L. Kang and Y.C. Luo, *New J. Chem.*, 37 (2013) 1105.
12. Y.T. Li, F. Fang, H.L. Fu, J.M. Qiu, Y. Song, Y.S. Li, D.L. Sun, Q.A. Zhang, L.Z. Ouyang and M. Zhu, *J. Mater. Chem. A*, 1 (2013) 5238.
13. Z.J. Gao, Y.C. Luo, Z. Lin, R.F. Li, J.Y. Wang and L. Kang, *J. Solid State Electrochem.*, 17 (2013) 727.
14. J.H. Zang, Q.A. Zhang, and D.L. Sun, *J. Alloys Compd.*, 771 (2019) 711.
15. L.Z. Ouyang, T.H. Yang, M. Zhu, D. Min, T.Z. Luo, H. Wang, F.M. Xiao and R.H. Tang, *J. Alloys Compd.*, 735 (2018) 98.
16. W. Lv, J.G. Yuan, B. Zhang and Y. Wu, *J. Alloys Compd.*, 730 (2018) 360.
17. M. Nowak, M. Balcerzak and M. Jurczyk, *Int. J. Hydrogen Energy*, 43 (2018) 8897.
18. M. Dymek, M. Nowak, M. Jurczyk and H. Bala, *J. Alloys Compd.*, 780 (2019) 697.
19. F.L. Zhang, Y.C. Luo, A.Q. Deng, Z.H. Tang, L. Kang and J.H. Chen, *Electrochem. Acta*, 52 (2006) 24.
20. K. Aoki, X.-G. Li and T. Masumoto, *Acta Metall.*, 40 (1992) 1717.
21. M.N. Guzik, B.C. Hauback and K. Yvon, *J. Solid State Chem.*, 186 (2012) 9.
22. Y.H. Zhang, P.P. Wang, W.G. Bu, Z.M. Yuan, Y. Qi and S.H. Guo, *RSC Adv.*, 8 (2018) 23353.
23. B. Li, J.D. Li, H.J. Zhao, X.Q. Yu and H.Y. Shao, *Int. J. Hydrogen Energy*, 44 (2019) 6007.
24. R.F. Li, J. Wan, F. Wang, C.P. Ding and R.H. Yu, *J. Power Sources*, 301 (2016) 229.

25. R.A. Young, The Rietveld Method, Introduction to the Rietveld Method; R.A. Young Eds.; Oxford University Press Inc; New York, 1995, p.1.
26. J. Rodriguez-Carvajal, Abstract of the Satellite Meeting on Powder Diffraction, Congress of IUCr, Toulouse, France, 1990, p. l27.
27. T. Ozaki, M. Kanemoto, T. Kakeya, Y. Kitano, M. Kuzuhara, M. Watada, S. Tanase and T. Sakai, *J. Alloys Compd.*, 446-447 (2007) 620.
28. F. Li, K. Young, T. Ouchi and M.A. Fetcenko, *J. Alloys Compd.*, 471 (2009) 371.
29. C.C. Yang, C. C. Wang, M.M. Li and Q. Jiang, *J. Mater. Chem. A*, 5 (2017) 1145.
30. L. Pauling, *J. Am. Chem. Soc.*, 54 (1932) 3570.
31. F.L. Zhang, Y.C. Luo, J.P. Chen, R.X. Yan and J.H. Chen, *J. Alloys Compd.*, 430 (2007) 302.